An egg image noise model for digital visual counting processing

Carlos Alberto Ramirez Behaine
Department of Electrical Engineering
University of Passo Fundo (UPF)
Rio Grande do Sul (RS), BR 285
Passo Fundo, 99052-900, Brazil
Email: cramireb@hotmail.com

Jaime S Ide
School of Medicine
Yale University
34 Park St, New Haven, 06519, USA
Email: jaime.ide@yale.edu

Abstract—Contactless counting is a suitable technique for the measurement of fragile commodities, acting as a successful tool for industrial production control. Visual counting processing is one of the most common contactless methods for non-invasive measurements. However, the creation of accurate models for processing images in realistic scenarios is still challenging due to the existence of noise in optical sensors. This paper proposes an egg image noise model for digital visual counting processing that incorporates particular aspects of real images in such acquisition systems. The matching function is defined in hue saturation value (HSV) color space, and a classical nearest neighbor cluster classification is utilized for the counting. Validation experiments are executed with low and high diversity test images, and the performance of the proposed model is compared to existing methods. The matching function results suggest that the introduced egg image noise model is able to represent more accurately complex aspects of egg images in an industrial environment. The comparative results show that the proposed model significantly improves digital visual counting, in terms of egg counting errors, and outperforms in 9% the second best method.

I. Introduction

Digital visual counting processing is a contact-less mechanism that can be required for minimal invasive measurements. Several visual measurement procedures take advantage of the imaging approach to achieve successful results in automatic visual object inspection [1], including egg counting and egg sizing for fecundity estimates [2], automatic counting of Aedes aegypti eggs utilizing segmentation [3], remote egg counting assistance [4], counting of silkworm eggs [5], chicken egg weight prediction and chicken egg size classification [6].

Chicken egg counting in industrial environments has evolved from mechanical contacts [7], weighing tools [8], and programmable electronic contacts to more recent visual approaches [9]. Modern computer vision and digital image processing tools [10] are widely used in industrial applications including chicken egg counting, especially because they are able to count eggs with high accuracy and speed, without direct human intervention [9]. However, one of the most difficult aspects of digital visual processing for egg counting in industrial environments is to deal with inadequate viewing angles and sensor noise.

There are several challenges for counting objects using digital images in industrial scenarios, such as image satura-tion, image noise, image shape distortions, and image feature extraction [11], [12]. Active shape modeling (ASM) is a promising approach for digital visual image processing due to its ability to handle cognitive problems in image interpretation [13], [14]. However, the model in ASM needs special points that are manually placed in a consistent training set of images. One key to the success of digital visual image processing is to utilize a complete set of images that are arranged and classified during the training stage. If this kind of set is no longer available in practice, the most powerful digital visual counting algorithm would not be operational [15]. The training set must have a good enough quality in order to ensure a balanced solution for the success of digital visual image processing [16]. As such, artificial imaging modeling representation is emerging for image shape prediction effects in some applications [17], [18].

This paper proposes an egg image noise model for digital visual counting processing that incorporates particular aspects of these images in an industrial environment. The core of this approach is based on 2D parametric functions that project egg shapes in color map representations, utilizing filtering and statistic models for positioning and noise representation. The proposed parametric model has the ability to represent realistic egg images for both the training and the inference counting processing, which is explained step by step in the next sections: Proposed model (section II), Experimental results (section III), and Conclusions (section IV).

II. Proposed model

The proposed egg image noise model for digital visual counting processing has two main steps. The fundamental step is the creation of the egg image noise model, where chicken egg shapes, distortions, and noise effects are parametrized (explained in sections II-A and II-B); and the second step is the model training, where optimal parameters are estimated utilizing a classical matching criterion on real egg images (explained in section II-C).

A. Egg image model

One of the state-of-the-art methods approximates the chicken egg shape with an elliptical form [6]. Since the

shape of a chicken egg is more complex and diverse than a simple ellipse, a model based on parametric projections is more adequate. Two dimensional (2D) parametric functions are traditional mathematical expressions that can represent different shapes [19]. Mathematical expressions can be rewritten in vector form with parametric functions, that is

$$f(x,y)^T = \Delta v_{a,k}{}^T , \qquad (1)$$

where $f(x,y)$ is the 2D egg shape parametric function with (x,y) coordinates, Δ is an orthogonal diagonal matrix and $v_{a,k}$ is an egg shape vector with a and k scalar parameters. The a parameter controls the circular-elliptical form and the k parameter scales the projection by axis, with $0 < a < 1$ and $0 < k < 1$. Eq. (1) can be rewritten as

$$f(x,y)^T = \underbrace{\begin{bmatrix} \sin(p) & 0 \\ 0 & \cos(p) \end{bmatrix}}_{\Delta} \underbrace{\begin{bmatrix} a\cos(kp) \\ -1 \end{bmatrix}}_{v_{a,k}{}^T} , \qquad (2)$$

where p is one among L possible angles between $-\pi$ and π, and $f(x,y)$ collects $2L$ elements from x and y axis projections.

The 2D egg shape parametric function in Eq. (2) needs to represent different sizes and rotations, thus, two mathematical operators are included in vector form, to make the proposed model more realistic. Therefore:

$$m(x,y)^T = S \times R \times f(x,y)^T , \qquad (3)$$

where $m(x,y)$ is the 2D egg shape model with (x,y) coordinates, S is the scale operation in a diagonal matrix form and R is the rotation operation in matrix form. Thus:

$$m(x,y)^T = \underbrace{\begin{bmatrix} s & 0 \\ 0 & s \end{bmatrix}}_{S} \underbrace{\begin{bmatrix} \cos(\theta) & -\sin(\theta) \\ \sin(\theta) & \cos(\theta) \end{bmatrix}}_{R} f(x,y)^T , \qquad (4)$$

where s is the scale parameter and θ is the angle of rotation, that can be visualized in Fig. 1 (a).

Digital color images are usually represented by the projection of three channels in 2D matrix representation [10]. Since the eggs have a variety of colors, a cognitive color space HSV (Hue Saturation Value) is selected to model the appearance of real eggs, and an RGB (Red Green Blue) color space is used for hardware visualization. Then, the color of egg surfaces is represented by

$$E(\acute{x}, \acute{y}) = F\{H_m(h, \zeta, \beta)\} , \qquad (5)$$

where $E(\acute{x}, \acute{y})$ is the foreground matrix of pixels with $(\acute{x}, \acute{y})$ coordinates in RGB color space channel included in the egg model $m(x,y)$, $H_m(h, \zeta, \beta)$ is the foreground matrix of pixels in HSV color space channel of an egg color image of interest with parameters: the hue (color) h, the color saturation ζ, and the value β. The HSV color space channel to RGB color space channel conversion is represented by the matrix operator $F\{\cdot\}$ [10].

The full image W in $(\dot{x}, \dot{y})$ coordinates, is composed by the union between the foreground pixels and the background pixels, that is

$$W = E(\acute{x}, \acute{y}) \bigcup \widehat{E}(\widehat{x}, \widehat{y}) , \qquad (6)$$

where $\widehat{E}(\widehat{x}, \widehat{y})$ are background pixels that are localized at the complement coordinates of $E(\acute{x}, \acute{y})$, and can be filled with a suitable color for egg color contrast. The foreground matrix of pixels $E(\acute{x}, \acute{y})$, from HSV parameters of a typical chicken egg: $h = 0.1056$, $\zeta = 0.3061$, $\beta = 0.9800$, is illustrated in Fig. 1 (b).
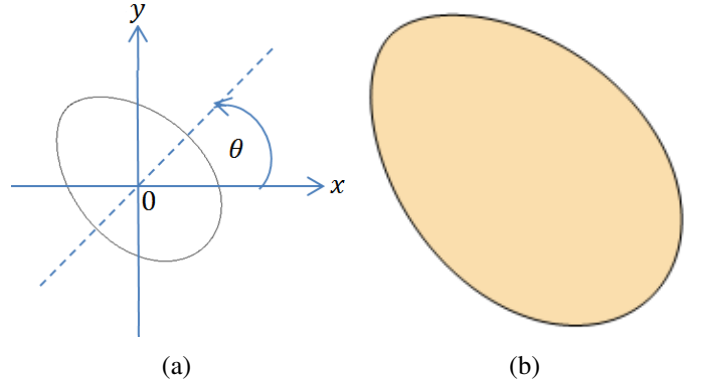

Fig. 1. (a) The 2D egg shape model $m(x,y)$ with $a = 0.72$, $k = 0.25$, $s = 0.7$ and $\theta = \pi/4$, (b) the foreground matrix of pixels $E(\acute{x}, \acute{y})$, from HSV parameters of a typical chicken egg: $h = 0.1056$, $\zeta = 0.3061$, $\beta = 0.9800$.

B. Egg image noise model

Realistic scenarios of egg images for visual counting are contaminated by several types of noise. Therefore, the proposed model is composed by a set of egg image noise models that are common in industrial environments [20]:

$$\mathcal{J} = \Lambda_\delta \left(G_{\mu,\vartheta} \left(M_\epsilon \left(\mathbf{G}_\sigma * W \right) \right) \right) , \qquad (7)$$

where $\mathbf{G}_\sigma$ is the 2D Gaussian filtering smoothing kernel matrix with standard deviation specified by σ, $*$ is the 2D convolution operator, $M_\epsilon(\cdot)$ is the multiplicative noise operator with uniformly distributed random noise with mean 0 and variance ϵ, $G_{\mu,\vartheta}(\cdot)$ is the Gaussian white noise with constant mean μ and variance ϑ, $\Lambda_\delta(\cdot)$ adds salt and pepper noise with δ pixel density, and $\mathcal{J}$ is the proposed egg image noise model.

$\mathbf{G}_\sigma$ simulates the smoothing effect of the focus camera delay due to the image motion. $M_\epsilon(\cdot)$ is utilized to describe the loss of color fidelity due to RGB channel interference into the image sensor. $G_{\mu,\vartheta}(\cdot)$ represents the image saturation and the Joule's effect that comes from electronic devices. $\Lambda_\delta(\cdot)$ simulates the impulsive sparse noise that comes from electrical switching present in industrial environments.

C. Matching error

The matching procedure compares the egg image noise model with the real egg image. The fundamental matching

error is based on the differentiable and classical mean squared error (MSE) in HSV color space [21], following the cumulative sum each color map of NxM pixels of the image:

$$\mathcal{F} = \mathcal{F}_h + \mathcal{F}_\zeta + \mathcal{F}_\beta \,, \tag{8}$$

$$\mathcal{F}_h = p_h \left\{ \sum_{\dot{x}=1}^{N} \sum_{\dot{y}=1}^{M} \frac{[I_h(\dot{x},\dot{y}) - \mathcal{J}_h(\dot{x},\dot{y})]^2}{(NM)} \right\} \,, \tag{9}$$

$$\mathcal{F}_\zeta = p_\zeta \left\{ \sum_{\dot{x}=1}^{N} \sum_{\dot{y}=1}^{M} \frac{[I_\zeta(\dot{x},\dot{y}) - \mathcal{J}_\zeta(\dot{x},\dot{y})]^2}{(NM)} \right\} \,, \tag{10}$$

$$\mathcal{F}_\beta = p_\beta \left\{ \sum_{\dot{x}=1}^{N} \sum_{\dot{y}=1}^{M} \frac{[I_\beta(\dot{x},\dot{y}) - \mathcal{J}_\beta(\dot{x},\dot{y})]^2}{(NM)} \right\} \,, \tag{11}$$

where $\mathcal{F}$ is the matching error between the image noise model $\mathcal{J}$ and the real image I in HSV color space, $\mathcal{F}_h$ is the hue color map matching with a weight of p_h, $\mathcal{F}_\zeta$ is the saturation color map matching with a weight of p_ζ, and $\mathcal{F}_\beta$ is the brightness value color map matching with a weight of p_β. The sum of the particular weights is unitary. The region of interest (ROI) was selected by threshold of pixels with high level of luminance. The best model parameters for the inference are selected by the minimal value of the matching error $\mathcal{F}$ during the training. The counting procedure is based on the classical nearest neighbor cluster classification, which is arranged in terms of the minimal values of the matching, expressed in Eq. (8). The most representative clusters are selected by the maximum local derivative value from the frequency of cluster elements, beginning from the minimal frequency values.

III. Experimental results

Two scenarios were tested: one scenario with low diversity of eggs (101 eggs in thirteen images) and another scenario with a high diversity of eggs (300 eggs in ten images). The hardware tool utilized was the Logitech HD webcam C270 (1280 x 720 pixels) and the software tool utilized was the GNU Octave with m-file scripts on an Intel Core i7-4770 processor with 32-GB RAM and 3.40-GHz frequency [22]. The proposed model was tested for matching (section III-A) and for counting processing (section III-B).

A. Matching results for egg image models

The selected scenario was composed by images that are contaminated by noise and distortion effects [9], [12]. The optimal image model was selected using the minimal value of the matching error during the training. Each image model was trained using 20 instances of parameters over one real image. The real image for training is illustrated in Fig. 2 (a), the optimal egg image noise model is illustrated in Fig. 2 (b), and the optimal egg image model is illustrated in Fig. 2 (c). The minimal matching error was achieved utilizing the egg image noise model in Eq. (7), which was $\mathcal{F} = 0.0699$, with the set of parameters: $\sigma = 1$, $\epsilon = 0.200$, $\mu = 0.160$, $\vartheta = 0.001$, $\delta = 0.00005$, in comparison with the results in
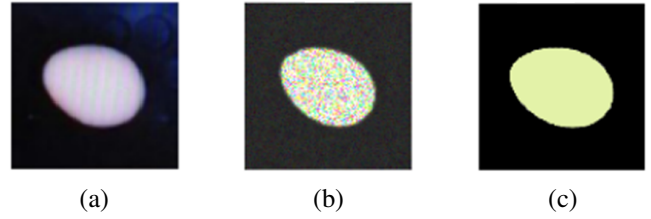

Fig. 2. (a) The real image for training, (b) the optimal egg image noise model in terms of the minimal matching error $\mathcal{F} = 0.0699$, and (c) the optimal egg image model in terms of the minimal matching error $\mathcal{F} = 0.1718$.

terms of the matching error $\mathcal{F} = 0.1718$, obtained with the egg image model in Eq. (6).

The results of the minimal matching error in Eq. (8) are visualized for the proposed model, for the real egg image and for the egg image model in Fig. (3) in the low diversity scenario. The comparative results in Fig. (3) show that in the low diversity scenario it is possible to obtain optimum matching results utilizing the proposed model. In this scenario, the image model without noise shows the worst matching results, in terms of matching error.
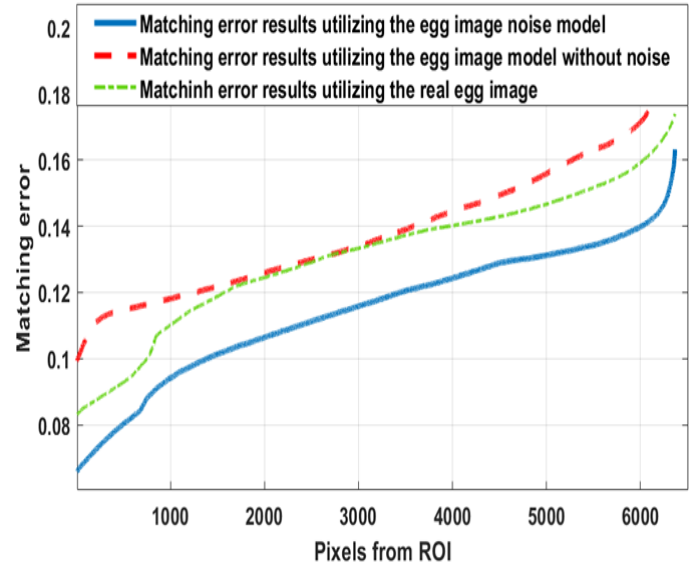

Fig. 3. Minimal matching error for the proposed model, for a real egg image and for the egg image model without noise in the low diversity scenario.

The procedure of counting follows the classical nearest neighbor cluster classification, which is arranged in terms of the minimal values of the matching error. The clustering results, in terms of frequency of pixels per cluster, utilizing the proposed model are visualized in Fig. (4) in the low diversity scenario.

The clustering results utilizing the proposed model over a test image are visualized in Fig. (5) in the low diversity scenario. The most representative clusters are selected by the maximum local derivative value from the frequency of cluster elements.
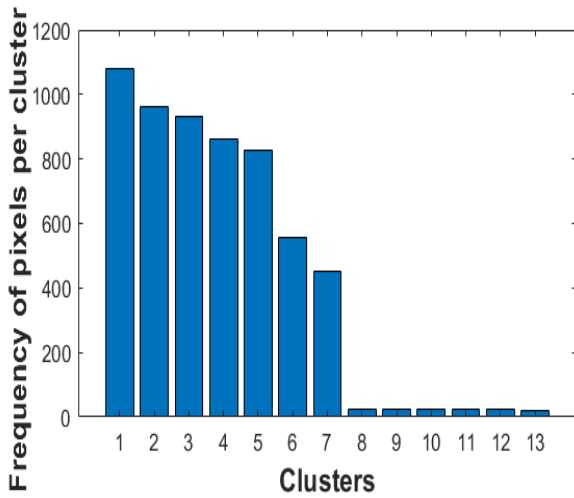
Fig. 4. The clustering results, in terms of frequency of pixels per cluster, utilizing the proposed model in the low diversity scenario.
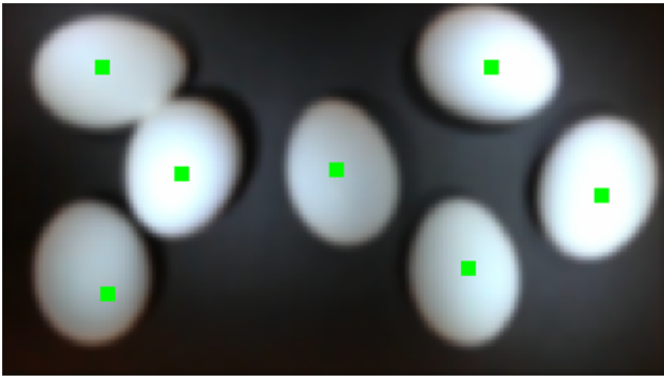

Fig. 5. The clustering utilizing the proposed model over a test image in the low diversity scenario.

The results of the minimal matching error in Eq. (8) are visualized for the proposed model, for the real egg image and for the egg image model in Fig. (6) in the high diversity scenario. In this scenario, both the image model without noise and the real egg image, show a few values of minimal matching error in some specific areas in the ROI. However, the complete comparative results in Fig. (6) show that in the high diversity scenario it is possible to obtain minimal overall error results utilizing the proposed model.

The procedure of counting follows the classical nearest neighbor cluster classification, which is arranged in terms of the minimal values of the matching error. The clustering results, in terms of frequency of pixels per cluster, utilizing the proposed model are visualized in Fig. (7) in the high diversity scenario.

The clustering results utilizing the proposed model over a test image are visualized in Fig. (8) in the high diversity scenario. The most representative clusters are selected by the maximum local derivative value from the frequency of cluster elements. The counting results in Fig. (8) shows that the false
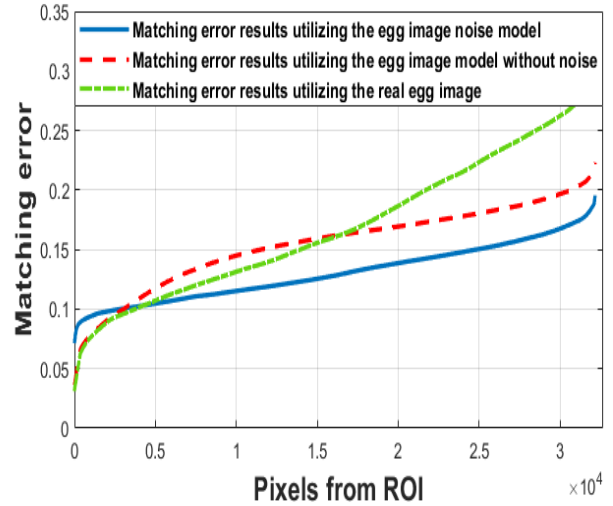

Fig. 6. Minimal matching errors for the proposed model, for a real egg image and for the egg image model without noise in the high diversity scenario.
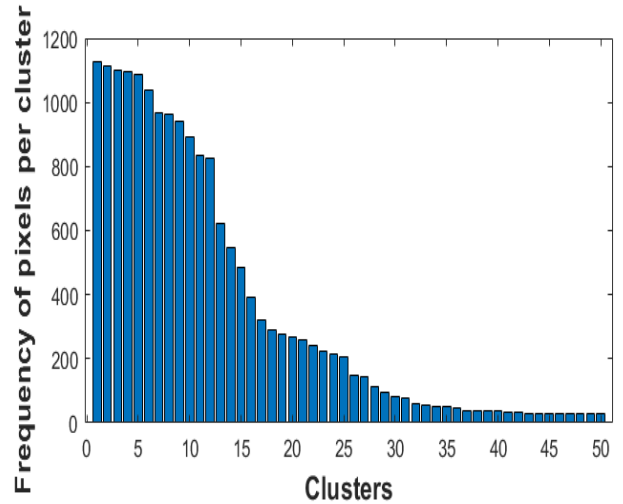

Fig. 7. The clustering results, in terms of frequency of pixels per cluster, utilizing the proposed model in the high diversity scenario.

positive is six and the false negative is three.

B. Comparison of digital counting processing methods

To reflect realistic scenarios in industrial environments, the test images did not have full control of illumination and anti-aliasing filtering. The low diversity scenario consists of 101 white chicken eggs (one type and similar size) in thirteen raw images. The high diversity scenario consists of 300 chicken eggs (five types and different sizes) in ten raw images.

The Table I presents the comparative performance evaluation of previous digital visual counting processing methods in [3], [9], and the proposed image noise model for both, low and high diversity chicken eggs, in terms of egg counting errors. The methods [9] and [3] both utilize statistical approaches in order to estimate the number of eggs in the image. Specifically,
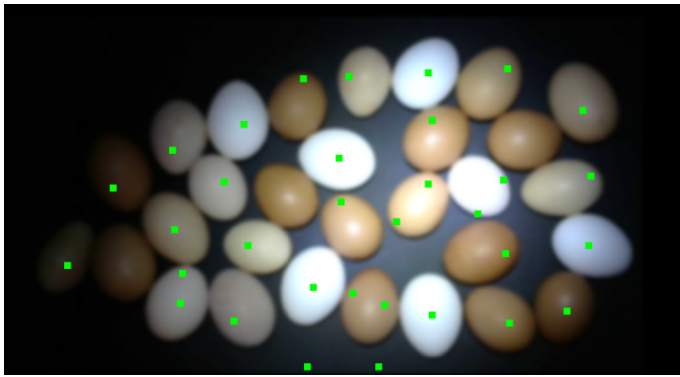
Fig. 8. The clustering utilizing the proposed model over a test image in the high diversity scenario.

Counting method tested	% of error in low diversity	% of error in high diversity
K-means clustering [3]	12.87%	39.33%
Global thresholding [9]	11.88%	30.33%
Model without noise	6.93%	27.33%
Real image template	0.00%	14.33%
Proposed model	0.00%	5.33%

in [9] the mean of the number of pixels for the expected size of the eggs is calculated using global threshold segmentation in a controlled lighting environment. The method showed in [3], the segmentation of the eggs in the foreground is done using YIQ color model (luminance Y, chrominance in-phase I and chrominance quadrature Q) in two ways: by limiarization with fixed thresholding and by binarization using k-means clustering method.

In the low diversity scenario, the method of global thresholding in [9] shows the performance result of 11.88% that is worse than the one described previously in the paper (0.2% in errors). This discrepancy is expected due to the fact that the method in [9] was tested with controlled illumination. For the method of k-means clustering in [3], the performance result is 12.87%, and worse than the ones in [9] (0.2% in errors), however it is expected due to the fact that the method in [3] was tested for Aedes aegypti eggs (7.84% in errors). On the other hand, the proposed method based on an image model without noise shows a performance result of 6.93%, and the proposed model that considers the noise effects achieves a performance result of 0% in terms of counting errors of chicken eggs. This is actually the same performance utilizing a real image as the template, with sizes and rotation operations, in the low diversity scenario. However, in the high diversity scenario, the proposed model is the only one to achieve a reasonable performance (5.33% in errors), as compared to the second best result using a real image as the template (14.33% in errors). The relative inference speed for the proposed egg image noise model for digital visual counting processing was 1716 times inferior to the faster method in real time at the high diversity scenario [9].

IV. CONCLUSION

The proposed egg image noise model for digital visual counting processing was introduced considering multiple aspects of realistic scenarios. Such aspects, related to the control of productivity in the industry of eggs, involved shapes, sizes, rotations, colors, appearance, and several types of noise from electrical devices in the image sensors. The matching results obtained in the validation experiments suggest a well–expected capability of the proposed image noise model, and the comparative results show that the egg image noise model improved performance, in terms of error of counting, in comparison with other digital visual counting processing methods. Specifically, it outperformed the second best model in 9% at the high diversity scenario. Finally, although the presented method, combining shape and noise modelling, focused on the counting of eggs, it could be naturally extended to other counting applications in industrial environments.

REFERENCES

[1] A. A. Khule, M. S. Nagmode, and R. D. Komati, "Automated object counting for visual inspection applications," in *2015 International Conference on Information Processing (ICIP)*, 12 2015, pp. 801–806, [doi:10.1109/INFOP.2015.7489491].

[2] K. Friedland, D. Ama-Abasi, M. Manning, L. Clarke, G. Kligys, and R. Chambers, "Automated egg counting and sizing from scanned images: Rapid sample processing and large data volumes for fecundity estimates," *Journal of Sea Research.*, vol. 54, no. 4, pp. 307 – 316, 2005, [doi:/10.1016/j.seares.2005.06.002].

[3] C. Mello, W. Dos Santos, M. A B Rodrigues, A. Candeias, and C. Gusmao, "Image segmentation of ovitraps for automatic counting of aedes aegypti eggs," vol. 2008, 02 2008, pp. 3103–6, [doi:10.1109/IEMBS.2008.4649860].

[4] M. Da Silva, M. A B Rodrigues, and R. de Araujo, "Aedes aegypti egg counting system," *Conference proceedings : ... Annual International Conference of the IEEE Engineering in Medicine and Biology Society. IEEE Engineering in Medicine and Biology Society. Conference*, vol. 2011, pp. 6810–2, 08 2011, [doi:10.1109/IEMBS.2011.6091679].

[5] S. S. Pathan and A. D. Harale, "Silkworm eggs counting system using image processing algorithm," in *Techno-Societal*, 12 2018, pp. 327–335, [doi:10.1007/978-3-319-53556-2 32].

[6] J. Thipakorn, R. Waranusast, and P. Riyamongkol, "Egg weight prediction and egg size classification using image processing and machine learning," in *2017 14th International Conference on Electrical Engineering/Electronics, Computer, Telecommunications and Information Technology (ECTI-CON)*, June 2017, pp. 477–480, [doi:10.1109/ECTICon.2017.8096278].

[7] B. Leopold, "Poultry cage having an automatic egg counting mechanism," Patent 2 827 875, March, 1958.

[8] C. Lokhorst and H. Vos, "An automatic egg weighing and counting system for detailed analysis and control of egg production," *Journal of Agricultural Engineering Research*, vol. 57, no. 2, pp. 137 – 144, 1994, [doi:10.1006/jaer.1994.1013].

[9] C. A. R. Behaine and L. Cataneo, "Electronic counter of eggs in real time through images - (contador eletrônico de ovos em tempo real através de imagens)," in *2017 XXVIII Regional Congress of Scientific and Technological Initiation in Engineering - (Congresso Regional de Iniciação Cientifica e Tecnologica em Engenharia) (CRICTE)*, vol. 2017, Nov. 2018.

[10] R. Gonzalez and R. Woods, *Digital Image Processing*, 4th ed. Pearson, 2018. [Online]. Available: https://books.google.com.br/books?id=0F05vgAACAAJ

[11] J. Garcia Arnal Barbedo, "A review on methods for automatic counting of objects in digital images," *IEEE Latin America Transactions*, vol. 10, no. 5, pp. 2112–2124, Sep. 2012, [doi:10.1109/TLA.2012.6362356].

[12] B. C. Jacquot, B. M. Bolla, and S. Maguire, "Hybrid approach to mean-variance and photon transfer measurement," in *Image Sensing Technologies: Materials, Devices, Systems, and Applications II*, N. K. Dhar and A. K. Dutta, Eds., vol. 9481, International Society for Optics and Photonics. SPIE, 2015, pp. 56 – 64, [doi:10.1117/12.2176115].

[13] T. Cootes, C. Taylor, D. Cooper, and J. Graham, "Active shape models-their training and application," *Computer Vision and Image Understanding*, vol. 61, no. 1, pp. 38 – 59, 1995, [doi:10.1006/cviu.1995.1004].

[14] D. O. Medley, C. Santiago, and J. C. Nascimento, "Deep active shape model for robust object fitting," *IEEE Transactions on Image Processing*, vol. 29, pp. 2380–2394, 2020, [doi:10.1109/TIP.2019.2948728].

[15] Y. Wang, Y. Zou, J. Chen, X. Huang, and C. Cai, "Example-based visual object counting with a sparsity constraint," in *IEEE International Conference on Multimedia and Expo (ICME)*, Jul. 2016, pp. 1–6, [doi:10.1109/ICME.2016.7552900].

[16] X. Huang, Y. Zou, and Y. Wang, "Example-based visual object counting for complex background with a local low-rank constraint," in *IEEE International Conference on Acoustics, Speech and Signal Processing (ICASSP)*, Mar. 2017, pp. 1672–1676, [doi:10.1109/ICASSP.2017.7952441].

[17] P. Singh and P. Singh, "Implementation of SPIHT and WDR algorithms for natural and artificial images using wavelets," in *Fourth International Conference on Computational Intelligence and Communication Networks)*, Nov. 2012, pp. 359–363, [doi:10.1109/CICN.2012.132].

[18] F. Caponio, A. Abba, N. Lusardi, and A. Geraci, "A digital system for artificial generation of images from radiation detectors," in *IEEE Nuclear Science Symposium and Medical Imaging Conference (NSS/MIC)*, Nov. 2014, pp. 1–5, [doi:10.1109/NSSMIC.2014.7431136].

[19] J. Stewart, *Calculus, 7th ed.* Belmont: Thomson, Brooks Cole, 2012.

[20] C. Boncelet, "Chapter 7 - image noise models," in *The Essential Guide to Image Processing*, A. Bovik, Ed. Boston: Academic Press, 2009, pp. 143 – 167, [doi:10.1016/B978-0-12-374457-9.00007-X].

[21] L. Shuhua and G. Gaizhi, "The application of improved hsv color space model in image processing," in *2010 2nd International Conference on Future Computer and Communication*, vol. 2, 2010, pp. V2–10–V2–13, [doi:10.1109/ICFCC.2010.5497299].

[22] J. W. Eaton, D. Bateman, S. Hauberg, and R. Wehbring, *GNU Octave version 6.3.0 manual: a high-level interactive language for numerical computations*, 2021. [Online]. Available: https://octave.org/doc/v6.3.0/